Electromagnetic antenna for power electronic modules : towards a real time electromagnetic characterization

Guillaume Viné, Paul-Etienne Vidal, Jean-Marc Diénot

Electromagnetic antenna for power electronic modules: towards a real time electromagnetic characterization

G. Vine[1], P.-E.Vidal[1], J.-M. Dienot [2]
[1] LGP EA1905, Ecole Nationale d'Ingénieurs, INPT, Tarbes, France
[2] LGP/Labceem, Université P. Sabatier, Tarbes, France
E-Mail: guillaume.vine@enit.fr

Keywords

«Near-Field», «Emission», «Radiation», «Power PCB», «Magnetic Sensor».

Abstract

This study deals with near-field probes integration onto power electronic modules for the magnetic field measurement. In this paper, electromagnetic disturbances characterization is investigated. A loop-antenna-type, its design and its modeling are detailed. The measurement obtained on a buck power converter are presented. An analysis of conducted currents within the power module is developed. Based on them, it is shown that the probe measurements allow recovering the characteristics and the distribution of the electromagnetic disturbances.

Introduction

New developments in power electronic design deals with power density, switching ranges and more generally with wide band gap semiconductors' integration. This trend accentuates the ElectroMagnetic Compatibility (EMC) issues. More precisely, high levels of conducted and radiated disturbances are concerned and can degrade the overall device efficiency [1]. As a way of consequence, from the design stage, it is often interesting to characterize these non-desired contributors.

Near Field (NF) techniques enable the development of non-intrusive sensors with high temporal and spatial resolution. The electric field measurement is ensured by monopole and dipole probes whereas loop probes are used for magnetic field measurement. In most applications, the sensors are associated with an external robotic arm to scan step after step the top surface of the Device Under Test (DUT). That gives access to electromagnetic cartography. Indeed the localization of EM radiation sources and the DUT currents estimation [2] are performed. The sensor efficiency depends on probe size, surface of DUT and resolution step of the scanning system. However, the main limitation of NF scanning technique is the time consumption to collect all the samples, especially in Power Printed Circuit Board (PPCB) and Hybrid 3D structures. Due to their large size and to the 3D top surface, the scanning step and time characterization of such measurement systems does not allow an "in situ" and real time measurements.

To reduce time costs of the magnetic field investigations, the integration of several loop antennas onto electronic modules has been studied previously [3], [4]. That represents a first approach of the "in-situ" magnetic field measurement. The interest to sense transient magnetic fields in real time, with the device in nominal and real activity was highlighted. In this study, the loop antennas integration is applied to a power electronic module. The objective is to improve the electromagnetic diagnosis of these modules.

Firstly, an antenna prototype is proposed and modeled over a wide frequency range. Secondly, the studied power device is presented and the electromagnetic disturbances inside it are detailed and modeled. Finally, the measurement done with the antenna prototype and what can be concluded from the measured signal analysis are presented.

Near field measurement for power electronic devices

Near field principle

In electrical circuits, the electromagnetic (EM) field exists due to current flows and potential variations. In power modules, it has been demonstrated that high currents and voltages associated with very short switching times cause wideband electromagnetic radiations until 1GHz [5].

Close to sources, magnetic and electric fields are decoupled and one of them is dominant: the magnetic field for current flows, the electric field for potential variations. This corresponds to the near field region defined by (1) with D the distance between source and antenna, f the signal frequency and v the speed of light through the propagation medium.

$$D < \frac{v}{2\pi f} \tag{1}$$

The near field measurement in power modules requires a high proximity to the emission sources. For instance, a 1GHz frequency signal through the vacuum, corresponds to *D=5 cm* limit distance. Antenna integration is well suited to this condition.

Loop antenna theory

As illustrated in Fig.1, an elementary magnetic probe corresponds to a conductive loop antenna. It operates on the principle of inductive coupling according to Lenz's law (2). The change of the magnetic flux Φ through the loop surface *S* induces an electromotive force *e* at its terminal. Obviously, the magnetic flux is linked to the radiated magnetic field $\vec{H}$.

$$e = -\frac{d\phi}{dt},\ \phi = \iint_S \mu\vec{H}.\vec{n}\,dS \tag{2}$$

If the loop radius is sufficiently small, the magnetic field can be considered homogeneous inside it. The electromotive force is so expressed by (3). A relation is established between the output voltage of the antenna and the normal component of the magnetic field at the antenna center H_{nO}.

$$e = j\omega \iint_S \mu H_n\,dS \approx j\omega\mu S * H_{nO} \tag{3}$$

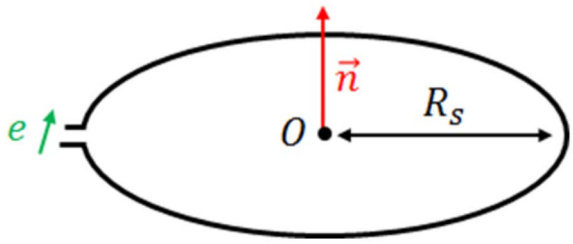

Fig.1: Elementary magnetic antenna.

The relation (3) requires 2 ideal assumptions about the antenna:

- The antenna is a punctual receiver [6];
- The antenna captures only the magnetic field [7];

That can induce errors during the measurement process. An analysis study on the technology, the design and the positioning of the antenna is essential in order to ensure the reliability of the measurement results. This study is not the purpose of this article. A kind of antenna circular form on FR4 epoxy substrate, presented in the following (Fig.3), is designed according to these considerations.

Near field magnetic coupling

In the case of integrated antennas inside an electrical circuit, the NF configuration allows establishing a link between the induced electromotive force and the magnetic field sources: the currents flowing in the circuit (4).

$$e(j\omega) = j\omega * \sum_{i=1}^{n} M_i(j\omega) * I_i(j\omega) \quad (4)$$

Where $I_i(j\omega)$ corresponds to the i[th] current and $M_i(j\omega)$ to the mutual inductance between the antenna and the propagation path of the i[th] current.

This principle is illustrated Fig.2. It includes the sources, the magnetic couplings and the magnetic antenna constituted by the conductive loop, the access lines and the measuring instrument represented by the termination load R_M [8]. Thus, in addition to the magnetic field measurement, the antenna loop can be used to estimate currents flowing in the circuit. The antenna integration will allow to recovering characteristics of the conductive electromagnetic disturbance.

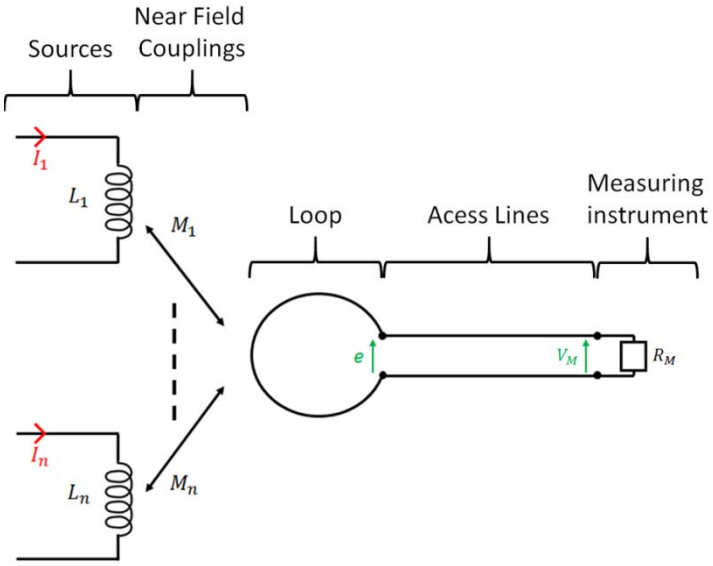

Fig.2: Coupling model of the antenna.

The measuring device accesses to the probe output voltage through access lines. They can influence the antenna response. The transfer factor is defined in (5). V_M corresponds to the voltage across the termination load and e the electromotive force induced in the magnetic loop:

$$F_t = \frac{V_M}{e} \quad (5)$$

Determination of F_t is essential to guarantee the efficiency of the magnetic measurement. The following part presents the modeling of the magnetic antenna prototype which enables the calculation of the transfer factor.

Antenna design and modeling

The antenna design corresponds to a circular form realized in planar technology, copper on epoxy substrate, with the following dimensions:

- The loop radius R_S=*3 mm* from the center of the loop to the middle of the trace
- The trace width of d_s =*0.2 mm* and the trace thickness of t_s =*0.2 mm*

The antenna is connected to measuring instruments through access lines and a SubMiniature version A–SMA connector of 50 *Ω* impedance. The dimensions of the access lines are L_A =*15 mm* length and the spacing from inner edges of Δ_L=*0.3 mm*. The prototype is shown in Fig.3.

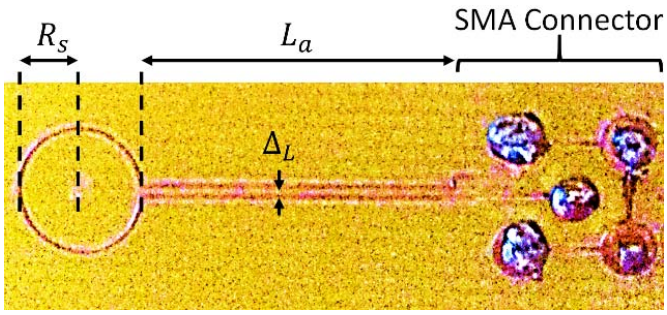

Fig.3: Real and designed antenna.

The transfer factor is computed in two steps. The first deals with antenna impedance model (Fig.4) and its experimental validation. The second step is about the transfer factor computation, based on the validated model. To validate the modeling, a Vector Network Analyzer (VNA) is used. It enables to measure the input impedance of the antenna.

We develop an equivalent lumped parameter model to determine the electrical characteristics of the antenna. To better match with the electrical behavior, the antenna is divided in 3 parts: loop, access lines and connector. Each part is depicted as an equivalent RLCG circuit. The common mode capacitors are inserted too (C_{mi}). Each parameter and coupling coefficients are extracted thanks to the software Q3D Extractor® depending of the frequency. The VNA is represented by the input voltage V_{in} and the termination load R_M=50Ω. The magnetic couplings are represented by the electromotive force *e*. The Fig.4 corresponds to a simplify representation of the lumped parameter model of the antenna. The description of the complete model is not the purpose of this paper. It is detailed in [9].

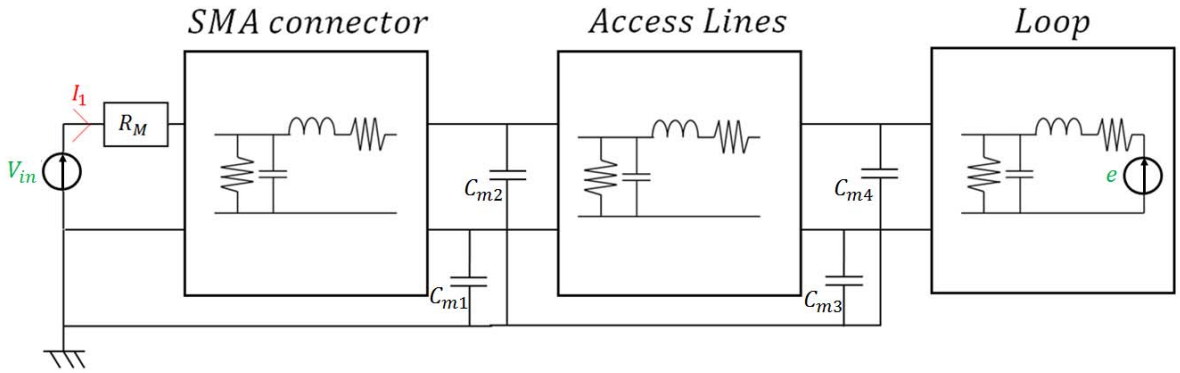

Fig.4: Lumped element model of the antenna.

The development of the circuit is transcribed in equation system based on the Kirchhoff's voltage laws. Each independent mesh corresponds to an equation. The input impedance of the antenna is deducted by the resolution of the system (6) where V_{in} is the input variable and the current I_1 the output variable. The electromotive force e is considered zero. Indeed, the input impedance is determined in the configuration of the antenna is isolated from external magnetic sources.

$$Z = \frac{V_{in} - R_{in} * I_1}{I_1} \tag{6}$$

The Fig.5 illustrates the comparison between computation and measurement of the antenna input impedance. A good agreement is obtained between the model and the measurement. The resonant frequency of the antenna is found at 1.02 GHz. Over this frequency, the probe no longer works as an inductive antenna. The magnetic field measurement is not effective due to the electric field captured. This corresponds to the limit measuring frequency of the antenna, in respect with the wideband electromagnetic radiations of power modules.

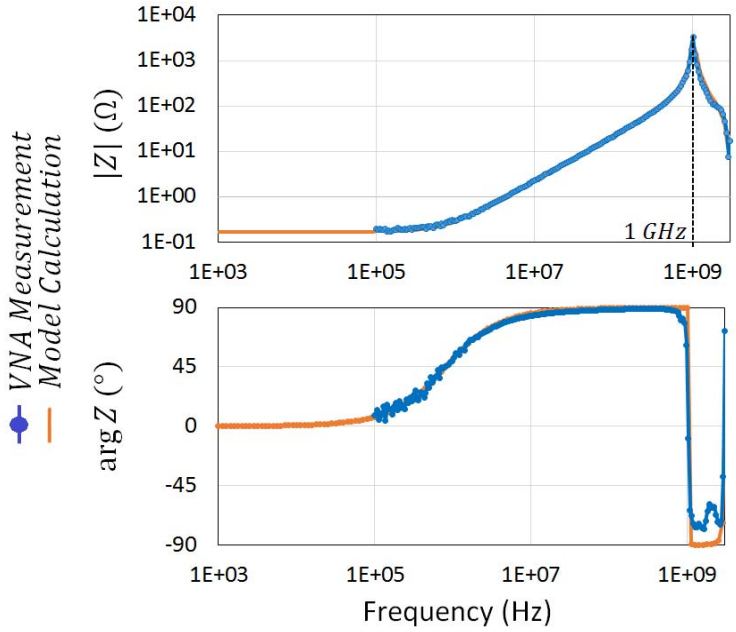

Fig.5: Comparison between the measured and calculated impedance of the antenna with e=0.

Thus, a wide frequency lumped element model of the antenna is established and experimentally confirmed. The transfer factor can be calculated. The antenna is considered in reception. The input voltage is now the electromotive force e induced by external magnetic field sources (3) and the measuring instrument voltage is considered zero. The transfer factor is deduced from (5) where V_M is the voltage across the termination load R_M and plotted in Fig.6.

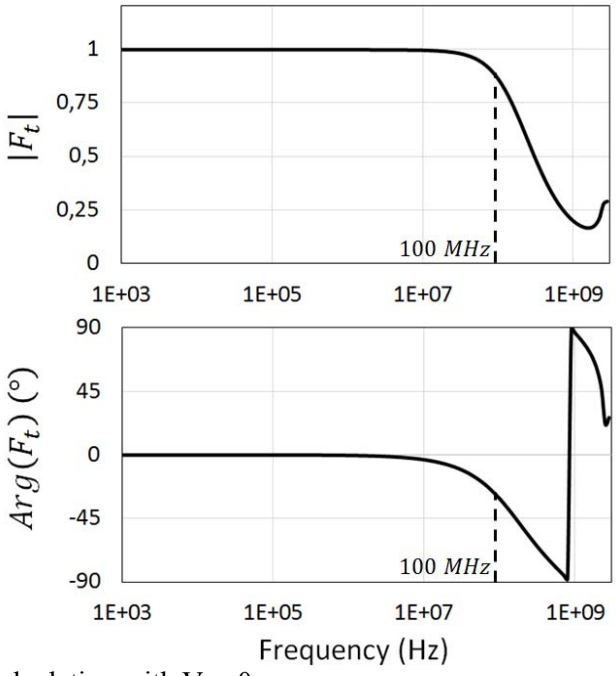

Fig. 6: Transfer factor calculation with V_{in}=0.

It is significant that the transfer factor is frequency constant over $1\,kHz < f < 100\,MHz$. In this condition, the output voltage of the antenna corresponds to electromotive force induced (7).

$$V_{out} = j\omega \iint_S \mu H_n \, dS \approx j\omega\mu S * H_{nO} \tag{7}$$

Over 100 MHz, the transfer factor is varying depending on the parasitic elements of the antenna and does not follow a frequency linear dependency. The measured signals by the probe onto the studied power module will be analyzed below this frequency in the following.

In this section, the design of a magnetic near field probe was presented. A lumped parameter model was developed and validated for a frequency span of 1 GHz. The transfer factor was computed and linearly defined below 100 MHz. The mastering of the probe electrical behavior allows us to consider the measurement of the magnetic field radiated by the studied power module.

Electromagnetic characterization of a power module

In this section, the power module for the integration of the magnetic probe and the measures done with it are presented.

Power electronics device

The studied device is a buck power converter for high temperature applications. This converter is specially developed internally in order to illustrate the in-situ near field probes capability. It is made of a silicon Insulated Gate Bipolar Transistor IGBT, associated in series with a silicon carbide diode. They are brazed on the top copper metallization of a Si_3N_4 ceramic substrate. The size of the substrate is 3*3 cm^2 whereas its nominal power can reach 8 kW. For our purpose, reduced voltage E=15 V and current I_{Load}=3 A are applied. The switching frequency of the IGBT gate signal is a 10 kHz square wave signal. A Line Impedance Stabilization Network (LISN) is used to filter electromagnetic disturbances from the network and to have a constant impedance at the input of the device. To ease the direct measurement of voltages and currents, neither plastic package nor silicone gel is used as illustrated Fig.7.

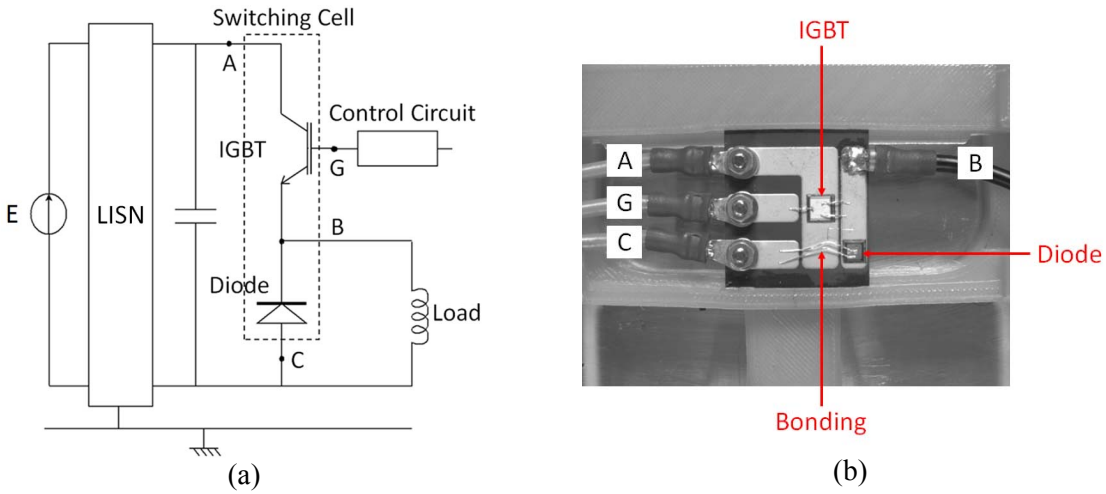

Fig.7: Power electronic demonstrator, (a) Equivalent electrical schema, (b) View of the switching cell.

The objective is the integration of magnetic antennas close to the switching cell. The output measurement should highlight the conductive. Indeed, the current paths are identified to finally lead to the radiated field. In this section an analysis of disturbance sources and paths is presented. It is inspired by the work done on a similar module [10] [11]. The model of the structure is linearized by substituting the switching cell with equivalent generators and their parasitic elements. The generators are voltage and current types, depending on the switching state. The initial proposed model is completed by the parasitic elements due to the load. Indeed, some complex current paths are finally identified.

Model of conductive electromagnetic disturbances

The EMI disturbance sources are identified to be the silicon devices that induce high voltage and current edges. Combined with parasitic R, L and C elements, they induce undesired high frequency oscillations. Two disturbance modes are distinguished, the common mode and the differential mode.
They are considered to be decoupled. They result from the current variation at the input of the converter, and the voltage variation at the terminals of the semiconductors, respectively. In the case of the common mode the place of the voltage generator is crucial. Indeed, it represents either the voltage

at the terminals of the IGBT, or the voltage at the terminals of the diode. The three distinguished configurations are described in Fig.8. The switching cell's parasitic elements, the load impedance and the LISN model have been added.

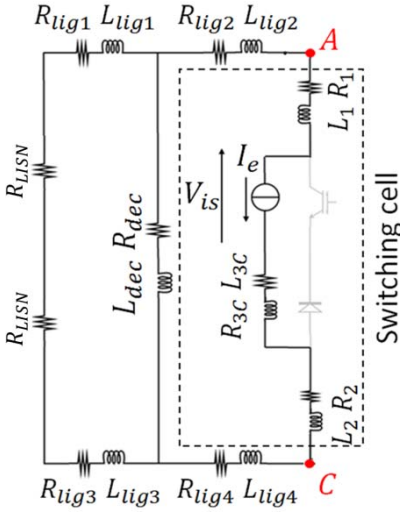

(a) Differential mode

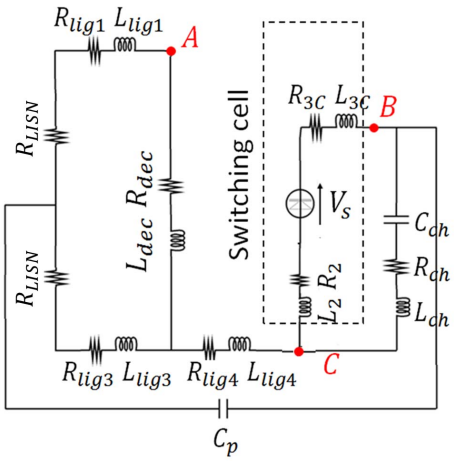

(b) Common mode 1 (IGBT switch off phase)

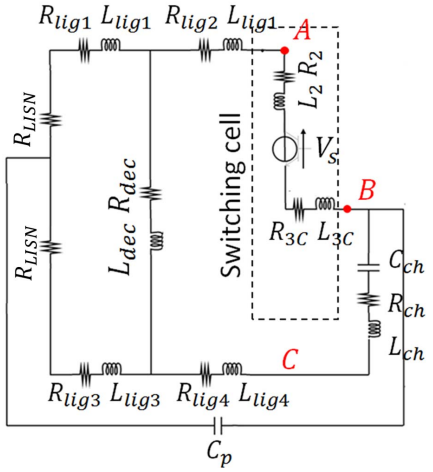

(c) Common mode 2 (diode switch off phase)

Fig.8: Common and differential mode, with their associated equivalent circuit model.

The choice of voltage source place is influenced by identifying the common mode disturbances propagation paths. Indeed, they are depending on the switching state of the transistor [12]. During the IGBT switch off phase, the disturbances are mainly propagated through the diode. As a matter of fact, the most suitable configuration is illustrated Fig.8.b. Conversely, when the diode switches off, the disturbances will mainly be transmitted through the IGBT, as depicted Fig.8.c. The two switching phases, the diode and the IGBT switching off, are thus distinguished in the case of the common mode because the sources of disturbance are distinct, respectively the IGBT and the diode.
Each path for disturbance propagation are thus exhibited and reported Fig.9:

- Path P1 : from pin named A to pin named C, associated to differential mode disturbances ;
- Path P2: from A to B, associated to common mode disturbances and the load resonance during diode switching off;
- Path P3: from pin B to C, associated to common mode disturbances and the the load resonance during diode switching off.

The positioning of the antenna at several points of the power module will allow to measure the different conductive disturbances.

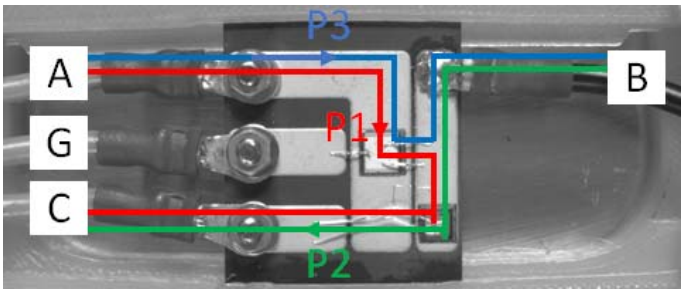

Fig.9: The three current paths of the switching cell.

Probe integration and experimental results

The magnetic antenna has been integrated onto the switching cell with a specific test support (Fig.10.a) at an elevation of 5 mm from the upper face of the device and oriented along the z-axis. The measurement is taken in 20 different positions detailed Fig.10.b. The output voltage of the antenna is monitored by an oscilloscope with a 800 ps time step. The input impedance of the oscilloscope is set at 50 Ω to insure the antenna characterization.

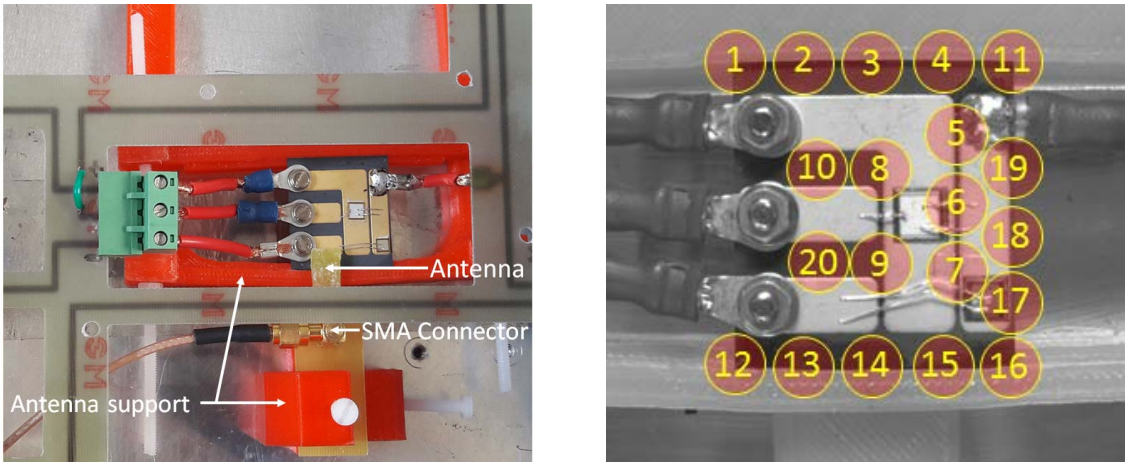

(a) (b)

Fig.10: (a) Magnetic field measurement bench with test support, (b) Points of measurement.

Based on the (7), the measured voltage of the antenna is linked to the normal component of the magnetic field H_Z at the antenna center. H_Z is firstly computed in the frequency domain by the direct Fourier Transform of the measured voltage and the use of the antenna transfer factor equal to $j\omega\mu S$ for frequencies below 100 MHz. Finally, the time domain signal is recovered from the inverse Fourier Transform. The Fig.11 illustrates the magnetic field measurement for different antenna positions.

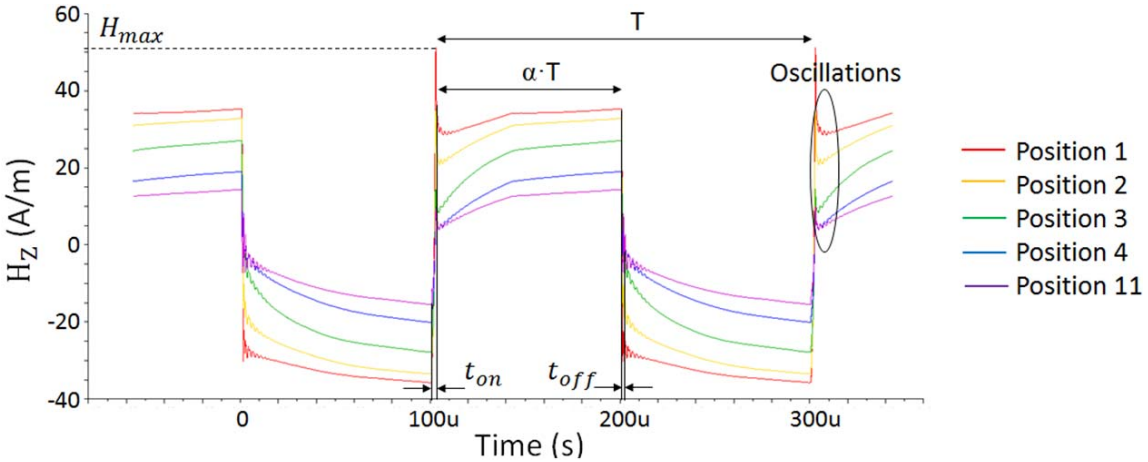

Fig.11: Magnetic field H_Z measurement at points 1, 2, 3, 4 and 11.

As explained previously, the magnetic field is an image of the currents flowing in the power module. The analysis of the temporal waveform of the signal measured provides information on the electrical behavior of the module. In Fig.11, the switching period $T = 10\,ms$, the duty cycle $\alpha = 0.5$, the switching times $t_{on} = 1.1\,us$ and $t_{off} = 0.38\,us$, and high frequency oscillations due to resonances of module parasitic elements are highlighted.

To analyze these oscillations, a zoom is made on the switching phases for the position 1 and 12 (Fig.12). Indeed, the antenna measures the radiated field induced by the current flowing through the pin A and C respectively. The comparison between gathered waveforms points out the disturbance sources.

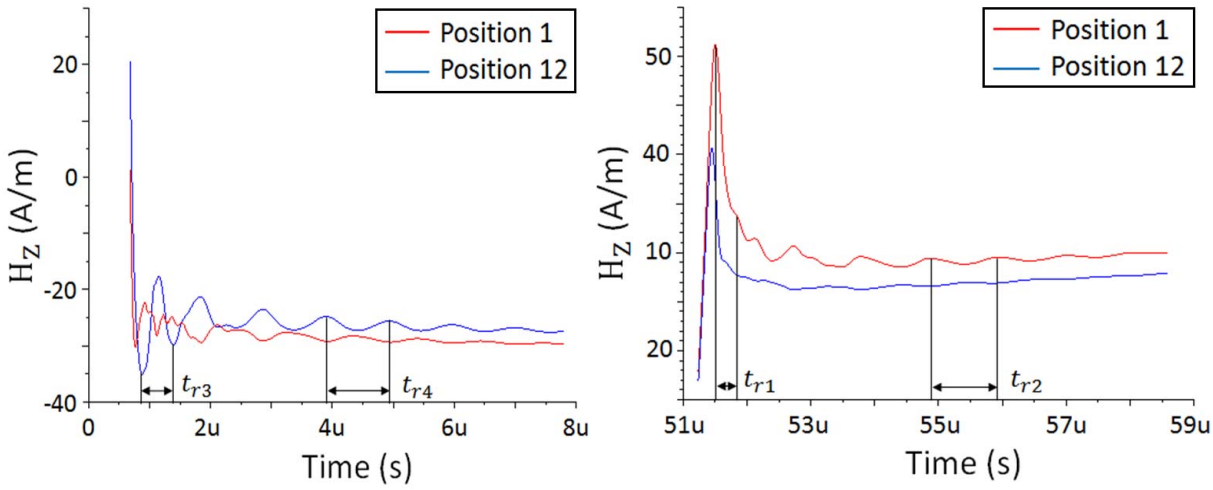

(a) IGBT switch off phase

(b) Diode switch off phase

Fig.12: Zoom view of the H_Z measurement at position 1 and 12 during switching phases.

Four pseudo-periods are firstly identified: $t_{r1} = 0.28\,us$, $t_{r2} = 1.3\,us$, $t_{r3} = 0.24\,us$ and $t_{r4} = 1.05\,us$. These oscillations are larger for the position 12 during the IGBT switch off phase and for the position 1 during the diode switch off phase. According to Fig.9, they can be associated to the conducted path 2 and 3. That allows to link them to the common mode resonance and the load resonance.

Another aim of the study is to monitor the magnetic field distribution in the module. For instance, the maximum magnetic field value obtained for each measuring point is reported Fig.13.

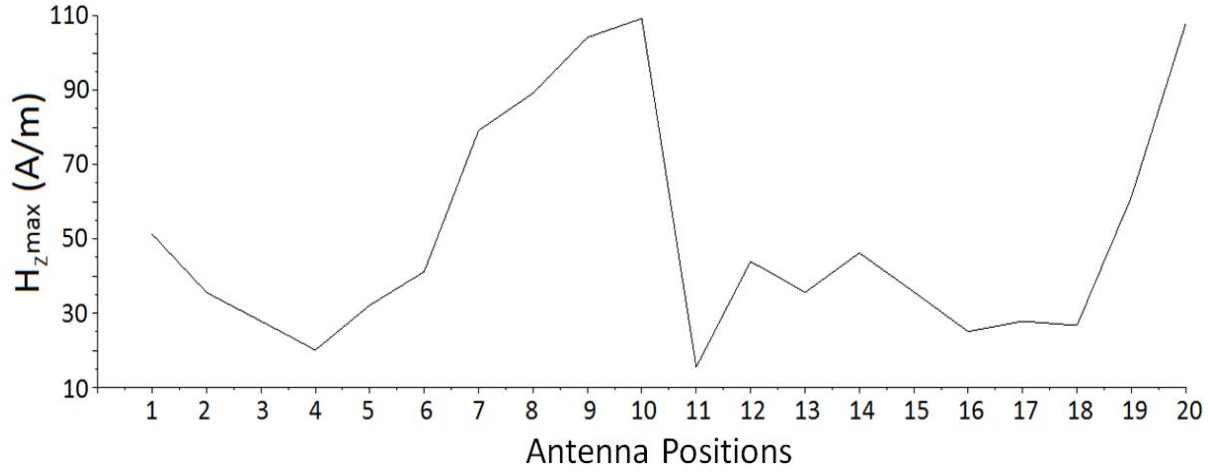

Fig.13: Maximum magnetic field values.

The magnetic hotspots correspond to the bonding wires proximity, positions 7 and 9, and to an absence of a ground plane behind the substrate - positions 8, 10 and 20. These results show the influence of the current paths of the switching cell (Figure 12) and the topology of the cell (Figure 13) on the magnetic field distribution. Thus, for both results, the analysis of the signals measured allows the electromagnetic disturbances characterization as well as the radiated magnetic field determination.

Conclusion

This study presents works to integrate magnetic antennas for “in situ” monitoring of power module. To achieve this objective, a loop antenna is realized in planar technology, copper on epoxy substrate. A lumped element model of the antenna is established and validated experimentally until 1 GHz. The measurement and simulation highlights an inductive linear behavior of the antenna on the frequency range above 100 MHz. The antenna response determined, its integration onto a high temperature power module is applied. Thus, with the use of the antenna, two main objectives are reached: the radiated field distribution over the module top surface and the conducted disturbance analysis. The information given by the integrated antennas would allow an optimization of the module design. Finally, it will ease the diagnostic of the EMC behavior of power modules.

References

[1] D. Boroyevich, X. Zhang, H. Bishinoi, R. Burgos, P. Mattavelli and F. Wang, "Conducted EMI and Systems Integration", *in Proceedings of 8th International Conference on Integrated Power Systems (CIPS),* pp. 1-14, Nuremberg, 2014.

[2] D. Baudry, A. Louis, and B. Mazari, "Overview of emission and susceptibility investigation and modeling with near-field measurements", *in Proceedings of XXIX General Assembly of the International Union of Radio Science (URSI)*, Chicago, 2008.

[3] J.M. Dienot and E. Batista, "EM-Matrix antenna for real-time measurements of electromagnetic noise in power electronic modules", *in Proceedings of Antennas & Propagation Conference,* pp. 753-756, Loughborough, 2009.

[4] G. Lourdel, J.M. Dienot, E. Dutarde, "Integrated Near-field probes for power switch Aln structure", Brevet FRA0405299, Mai 2004, International Patent Extension, USA, June 2005.

[5] R. Redl, "Electromagnetic environmental impact of power electronics equipment," *in Proceedings of the IEEE*, vol. 89, no. 6, pp. 926-938, Jun 2001.

[6] S. Iskra and I. P. MacFarlane, "H-field sensor measurement errors in the near-field of a magnetic dipole source", *in IEEE Transactions on Electromagnetic Compatibility*, vol. 31, no. 3, pp. 306-311, Aug 1989.

[7] H. Funato and T. Suga, "Magnetic near-field probe for GHz band and spatial resolution improvement technique", *in in Proceedings of 17th International Zurich Symposium on Electromagnetic Compatibility*, Singapore, pp. 284-28, 2006.

[8] G. Vine, J.-M. Dienot, P.-E. Vidal, "Theoritical and Experimental Study of Magnetic Sensors for Near-Field Emission Measurement", *in Proceedings of International Symposium on Electromagnetic Compatibility - EMC Europe*, Angers, 2017.

[9] M. Ishii and K. Komiyama, "A Measurement Method for the Antenna Factor of Small Loop Antenna by Measuring the Input Impedance", *in Proceedings of Conference on Precision Electromagnetic Measurements*, London, pp. 80-81, 2004.

[10] P. R. Mugur, J. Roudet and J. C. Crebier, "Power electronic converter EMC analysis through state variable approach techniques", *in IEEE Transactions on Electromagnetic Compatibility*, vol. 43, no. 2, pp. 229-238, May 2001.

[11] J. Meng, W. Ma, Q. Pan, L. Zhang and Z. Zhao, "Multiple Slope Switching Waveform Approximation to Improve Conducted EMI Spectral Analysis of Power Converters", *in IEEE Transactions on Electromagnetic Compatibility*, vol. 48, no. 4, pp. 742-751, Nov. 2006.

[12] C. Marlier, "Modélisation des perturbations électromagnétiques dans les convertisseurs statiques pour - des applications aéronautiques", Phd thesis, Ecole Centrale de Lille, 2009.